IEEE Journal of Microwaves

Received 22 March 2024; revised 7 June 2024; accepted 27 June 2024.

Digital Object Identifier 10.1109/JMW.2024.3421535

Switchless Multi-Octave Tune-All BPF Manifold Using Low-Pass/High-Pass Diplexer Junctions

MOHAMMED R. A. NASSER (Graduate Student Member, IEEE)
AND DIMITRA PSYCHOGIOU (Senior Member, IEEE)

Tyndall National Institute, University College Cork, T12 R5CP Cork, Ireland

CORRESPONDING AUTHOR: Mohammed R. A. Nasser (e-mail: mohammed.nasser@tyndall.ie).

This work was supported by the Defense Advanced Research Projects Agency (DARPA).

ABSTRACT This paper presents an RF-switchless two-bandpass filter (BPF) manifold with continuous multi-octave center frequency (f_{cen}) and bandwidth (BW) tuning capabilities that are demonstrated in a wide range of frequency range 1 (FR1) bands, spanning from L-band to C-band. Specifically, the proposed RF filtering component operates in three distinct modes of operation, namely: i) single-band, ii) dual-band, and iii) all-reject—achieved by intrinsically switching ON/OFF its two BPF branches. It is based on two tune-all BPFs that are combined with two high-pass/low-pass RF diplexer-based filtering junctions. A technique to minimize insertion loss (IL) using varactors and high-Q static DC block capacitors is demonstrated. The experimental prototype exhibits: i) a single-band mode of operation with f_{cen} tuning between 1.89–7.28 GHz, BW tuning ratio of 3–4.4:1 and minimum in-band insertion loss (IL): 2.3–5.7 dB), ii) a dual-band mode of operation with two independently tuned bands, and iii) an all-reject mode of operation with isolation < 15 dB between DC and 18 GHz.

INDEX TERMS Tunable filter, Band-pass filter (BPF), dual-band, reconfigurable filter, high-frequency filter, octave tuning.

I. INTRODUCTION

Adaptive RF filters will be key for the next generation of communications where dynamic utilization of the RF spectrum will be required to maximize spectral efficiency [1]. Additionally, they have the potential to reduce the deployment costs of new applications through RF hardware re-use. The next generation of RF filters should have multiple levels of RF tuning that go beyond center frequency tuning (f_{cen}). However, the majority of the existing electronically-tunable bandpass filters (BPFs) technologies have limited capabilities, namely f_{cen} tuning ratio (TR) up 2:1, bandwidth (BW) TR up to 2:1 and operational frequencies up to 1–3 GHz [2], [3], [4], [5], [6], [7], [8]. Thus, making them inadequate to cover the 5G+ expansions within the entire frequency range 1 (FR1) band (0.41–7.125 GHz).

The maximum tuning range of a BPFs is limited by the capacitance ratio of the varactor and its relation to the total capacitance of the resonator. To overcome this limitation, manifolds comprising multiple RF-switched filters are recently being considered as for example the ones in [9], [10], [11], [12]. However, they are based on lossy RF switches or PIN diodes that increase the RF front-end complexity and power consumption, introduce additional loss to each of the filtering channels (e.g., 1.8 dB for SOI switches [14]) and have limited transfer function (TF) adaptivity. For example, in [9], [10], [11], only f_{cen} tuning is achieved in a 4.4:1 tuning range by incorporating two or three RF-switched f_{cen}-tunable BPFs in the manifold. However, the resulting manifold is fairly large in size, its BW can't be tuned and its operational frequencies are limited to 2.4 GHz. In [12], 2.1:1 f_{cen} TR is achieved up to 3.9 GHz alongside 2.5-3:1 BW tuning, however its passbands exhibit high loss up to 9 dB. Furthermore, these manifolds are restricted in operation to a single band at a time.

Considering the aforementioned limitations, this manuscript reports for the first time a novel RF-switchless integration scheme for BPF manifolds. It utilizes two tune-all

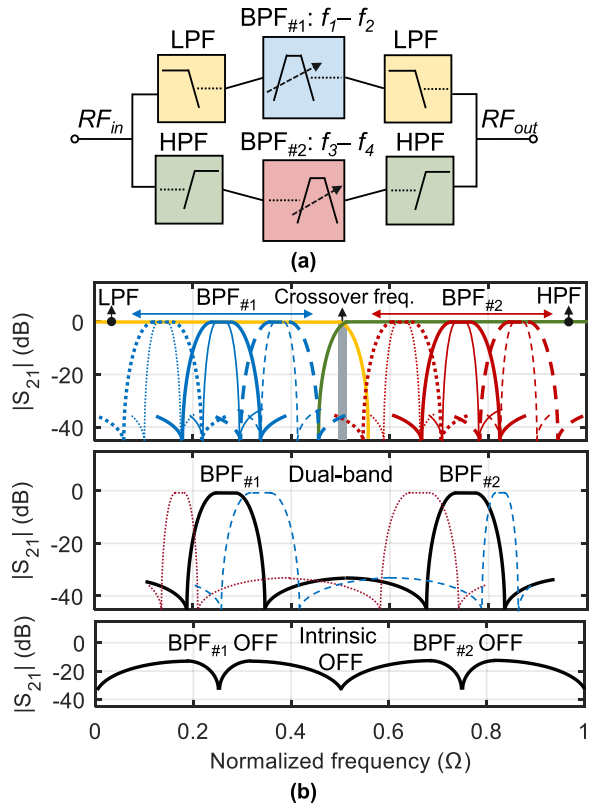

FIGURE 1. **RF-switchless two-BPF manifold using a high-pass/low-pass diplexer junction: (a) Block diagram; (b) Conceptual power transmission response exhibiting a tune-all transfer function with: i) a single-band mode featuring ultra-wide and continuous f_{cen} and BW tuning (either $BPF_{\#1}$ and $BPF_{\#2}$ is ON), ii) a dual-band mode with independently-tuned bands in terms of f_{cen} and BW (both $BPF_{\#1}$ and $BPF_{\#2}$ are ON), and iii) an all-reject mode (both $BPF_{\#1}$ and $BPF_{\#2}$ are intrinsically-switched OFF).**

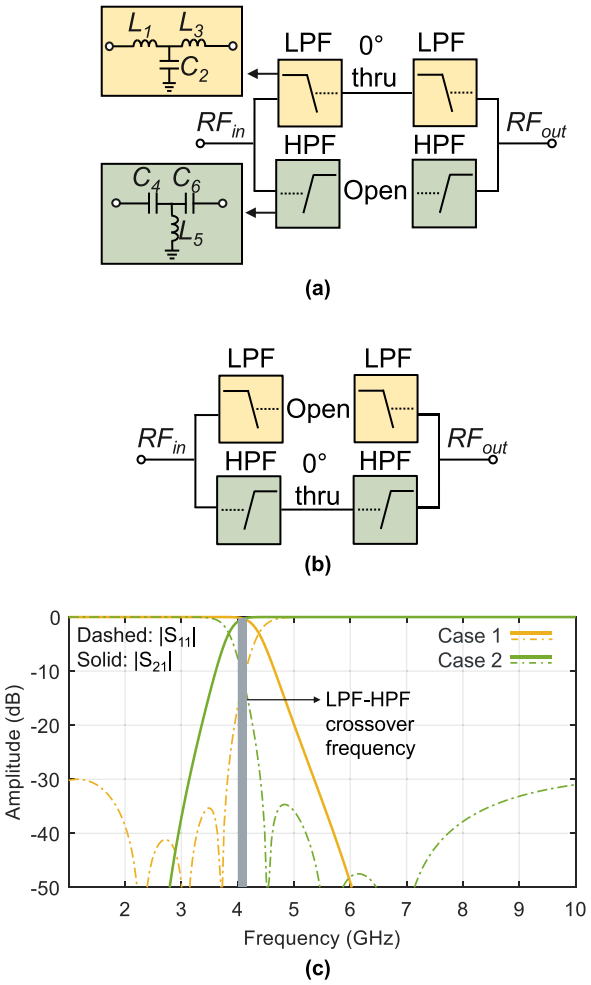

FIGURE 2. **Low-pass/ high-pass diplexer in back-to-back configuration: (a) Case 1: LPFs: directly connected, HPFs: open. (b) Case 2: HPFs: connected, LPFs: open; (c) Circuit simulations: LPF: $L_1 = 3.04$ nH, $C_2 = 1.44$ pF, $L_3 = 1.79$ nH, HPF: $C_4 = 0.52$ pF, $L_5 = 1.1$ nH, $C_6 = 0.88$ pF.**

BPFs—i.e., having multi-configurable TF parameters, including f_{cen} tuning, BW tuning and intrinsic RF switch-OFF—interconnected with two low-pass/high-pass RF diplexer junctions and exhibiting three distinct modes of operation, namely: i) a single-band TF with continuous f_{cen} tuning between 1.89-7.28 GHz corresponding to a TR: 3.85:1 and BW tuning 3-4.4:1), ii) a tunable dual-band mode of operation with two independently-tuned bands, and iii) an all-reject mode of operation spanning across a wide range of FR1 frequencies. As an important advantage to be highlighted, these modes are achieved by intrinsically switching ON/OFF the BPF branches without using any RF switches and only by tuning their resonators.

II. THEORETICAL FOUNDATIONS

A. CONCEPT OF THE RF SWITCHLESS MANIFOLD

Fig. 1 depicts the block diagram and the conceptual power transmission response of the switchless tune-all BPF manifold. It consists of: i) two diplexer junctions comprising a low-pass filter (LPF) and a high-pass filter (HPF), whose combined response is shown in Fig. 2 and ii) two fully-reconfigurable five-pole/two-transmission zero (TZs) BPFs ($BPF_{\#1}$ and $BPF_{\#2}$) with tune-all TF characteristics. The tuning capabilities of one of these BPFs are illustrated in Fig. 3 for the example case of $BPF_{\#1}$. They include f_{cen} tuning, BW tuning and intrinsic switching OFF. In the manifold configuration in Fig. 1, $BPF_{\#1}$ operates through the LPF channel with a continuously tunable TF between f_1 to f_2, while $BPF_{\#2}$ operates through the HPF channel with a continuously tunable TF between f_3 to f_4. By intrinsically switching ON/OFF the $BPF_{\#1}$ or the $BPF_{\#2}$, continuous f_{cen} and BW tuning between f_1 and f_4 can be obtained. A crossover region is considered between the LPF and HPF channels to allow for continuous f_{cen} coverage. Furthermore, the manifold facilitates two additional modes of operation. Specifically, by intrinsically switching ON both of the BPFs a dual-band mode can be achieved. Conversely by intrinsically switching OFF both of the BPFs an all-reject mode is materialized.

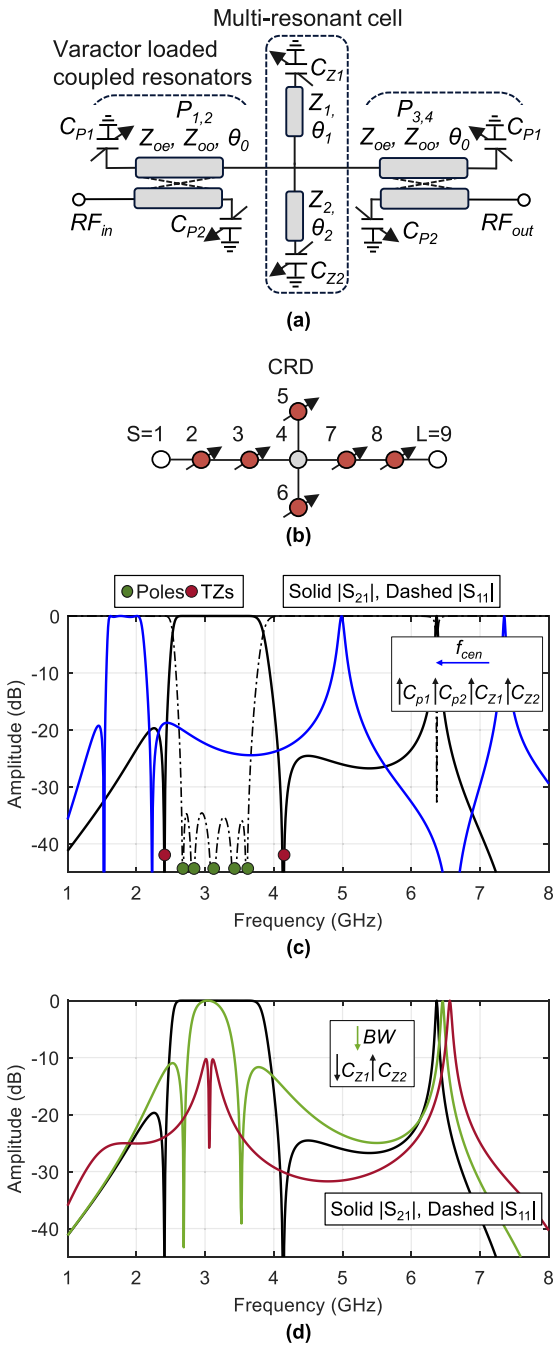

FIGURE 3. **(a) Five-pole/two-TZ BPF comprising four varactor-loaded coupled resonators and one multi-resonant cell; (b) Coupling routing diagram; (c) f_{cen} tuning, circuit-simulated response in black with f_{cen} = 3 GHz, FBW = 44% obtained for Z_{oe} = 180 Ω, $Z_{oo} = Z_{oe}/2$ Ω, θ_0 = 62°, Z_1 = 117 Ω, θ_1 = 87.8°, C_{Z1} = 0.2 pF, Z_2 = 123 Ω, θ_2 = 41.6°, $C_{P1} = C_{P2} = C_{Z1} = C_{Z2}$ = 0.2 pF; (d) BW tuning.**

B. IMPLEMENTATION

Using as a basis the aforementioned concept, the RF switchless tune-all BPF manifold is designed for f_{cen} tuning between 1.9 GHz–7.3 GHz, BW tuning > 3:1, FBW > 6%, a dual-band and an all reject mode of operation. To meet these design goals, $BPF_{\#1}$ is implemented for f_{cen} tuning between 1.9–3.9 GHz, whereas $BPF_{\#2}$ for f_{cen} tuning between 3.8–7.3 GHz. Both BPFs are realized for a BW TR: 3:1 and wide FBWs > 6%. To accommodate their switchless integration, the LPF/HPF diplexer is designed in a back-to-back configuration using third-order LPF/HPF channels considering two design cases: i) Case 1: LPFs directly connected (via a zero-length thru line), HPFs open-ended, and ii) Case 2: HPFs directly connected and LPFs open-ended. In contrast to conventional RF diplexers designed for 50 Ω terminations [13], alternative zero-length thru and open circuit interconnection terminations are considered when the diplexer junction is designed in a back-to-back configuration as shown in Fig. 2(a), (b). In Fig. 2(a), the two LPFs are cascaded via a zero-length thru line while the other two HPFs are open-circuited, and in Fig. 2(b), the two HPFs are cascaded via a zero-length thru line while the other two LPFs are open-circuited. The values of the lumped-element (LE) components for the diplexer are specified using optimized g-coefficients (g_1 = 1.527, g_2 = 1.813, g_3 = 0.9, $g_0 = g_4$ = 1) at f_c = 4 GHz ($\omega_c = 2\pi \cdot f_c$) and the following formulas: $L_1 = (Z_0 \cdot g_1)/\omega_c$, $C_2 = g_2/(Z_0 \cdot \omega_c)$ F, $L_3 = (Z_0 \cdot g_3)/\omega_c$ H *and* $C_4 = 1/(Z_0 \cdot g_1 \cdot \omega_c)$ F, $L_5 = (Z_0)/(g_2 \cdot \omega_c)$ H, $C_6 = 1/(Z_0 \cdot g_3 \cdot \omega_c)$ F for a return loss (RL) > 30 dB, where f_c is the centre of the crossover region at which the power transmission is transferred from the LPF channel to the HPF channel when arranged in a back-to-back and terminated to Z_0 = 50 Ohm. The ideal circuit-simulated S-parameters for Case 1 and Case 2 are provided in Fig. 2(c). As shown, the LPF channel spans between DC-4.34 GHz and covers the desired specifications of $BPF_{\#1}$, while the HPF starts from 3.7 GHz and covers the desired specifications of $BPF_{\#2}$. An overlapping cross over frequency range between 3.7 GHz (3 dB cut-off of the HPF) and 4.34 GHz (3 dB cut-off of the LPF) is considered to allow for continuous f_{cen} tuning.

It should be noted that $BPF_{\#1}$ and $BPF_{\#2}$ of the manifold implement the same type of TF [Fig. 3(a)], however shifted in frequency. Their TF comprises five poles and two transmission zeros (TZs) as shown in Fig. 3(c) alongside its coupling routing diagram [Fig. 3(b)]. In practice each of the BPFs is realized with two varactor-loaded coupled resonators contributing to four poles and a multi-resonant cell contributing to one pole and two TZs. The simulated S-parameters in Fig. 3(c), (d) illustrate tuning principles of the BPF TF. Specifically, i) f_{cen} shifts to lower frequencies by increasing all capacitances loading the resonators (C_{p1}, C_{p2}, C_{Z2}, *and* C_{Z2}) [Fig. 3(c)], ii) BW decreases by decreasing C_{Z1} and increasing C_{Z2} (tuning TZs to the center of the passband) [Fig. 3(d)], and iii) intrinsic-OFF is achieved by decreasing C_{Z1} and increasing C_{Z2} until both of the TZs are set at the center of the passband, and by offsetting the capacitances C_{p1} and C_{p2} in the varactor-loaded coupled line [Fig. 3(d)]. These principles are also outlined in [12]. However, two additional poles are introduced in this concept by altering the coupling between the varactor-loaded coupled resonators to widen the BPF's fractional bandwidth (FBW), achieving up to 44%, as opposed to 7.3% in [12].

The performance of BPFs is linked to the varactor's loss and tuning range. For high frequency implementations it is

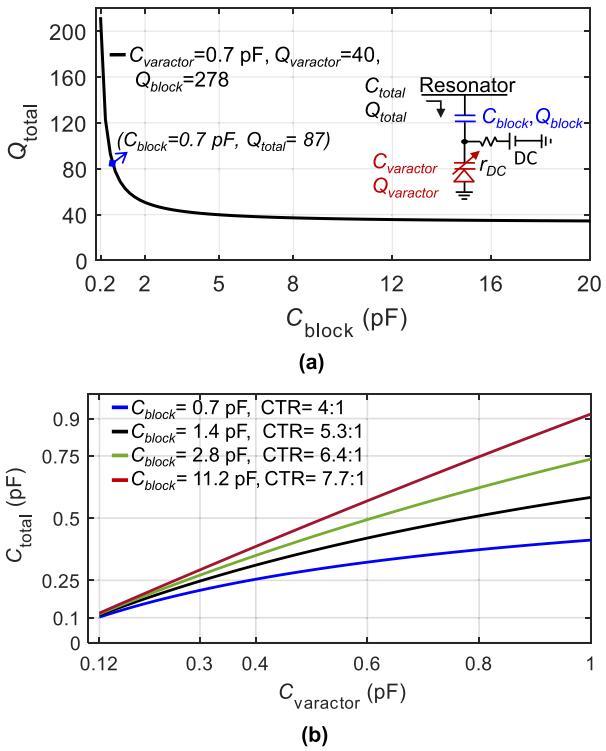

FIGURE 4. DC block effect on: (a) Q_{total}. (b) $C_{varactor}$ and C_{total}.

also influenced by the DC block capacitance (C_{block}) in its biasing network. Thus, a study of the C_{block} impact on the total unloaded quality factor (Q_{total}) and total capacitance tuning range (CTR) is illustrated in Fig. 4. Specifically, Fig. 4(a) demonstrates the effect of C_{block} while maintaining the varactor diode capacitance (C_{varactor}) and Q-factor ($Q_{varactor}$), and the DC block Q-factor (Q_{block}) constant. As observed, when C_{block} is comparable to C_{varactor}, Q_{total} rises and is comparable to Q_{block}, indicating that a low C_{block}, comparable to C_{varactor}, increases Q_{total}. Furthermore, Fig. 4(b) demonstrates that lowering C_{block} limits the CTR of the resonator. Thus, the DC block selection is based on a trade-off between Q-factor and capacitance tuning.

To analyse the varactor performance before designing the BPFs, a varactor-loaded resonator was manufactured as shown in Fig. 5(a) and tested between 2–5 GHz. MACOM MAVR-000120-14110G varactor diodes (with total capacitance C_t = 0.128–1.1 pF and Murata DC block capacitors were used. Its measured performance in terms of applied DC voltage and extracted unloaded Q-factor (Q_U) is provided in Fig. 5(b); and Fig. 5(c) illustrates its measured performance in terms of applied DC voltage and center frequency tuning. The results show that a lower capacitance DC block enhances the resonator's Q_U [Fig. 5(b)] but limits the TR of the center frequency [Fig. 5(c)]. This agrees well with the theoretical study in Fig. 4, successfully validating the proposed design method.

Having specified the varactor and resonator performance trade-offs, the manifold can be designed as follows. First the

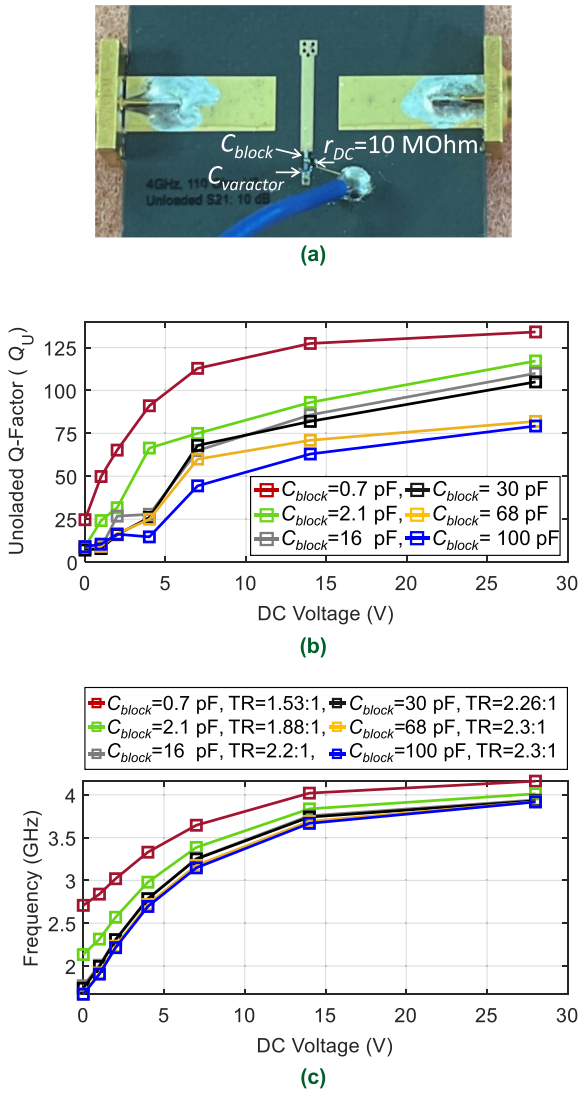

FIGURE 5. Experimental evaluation of the effect of the DC block on the unloaded Q-factor (Q_U) and tuning range of the varactor-loaded resonator: (a) Photograph of the manufactured c resonator. The utilized SMDs and resonator's characteristics are as follow: Varactor: MACOM MAVR-000120-14110G, DC blocks: GJM0335 and GRM0335 Murata series. Resonator characteristic: impedance $Z = 109\ \Omega$, electrical length: 55°at 4 GHz, substrate: RO5880 with a height of 1.575 mm; (b) Relationship between applied DC voltage and extracted Q_U; (c) Relationship between center frequency, where TR is the frequency tuning ratio. .

BPFs and the diplexers are designed independently. Afterwards the diplexers are optimized for realistic loads. i.e., the open circuit is replaced by the corresponding BPF in its intrinsically switched-OFF state and the thru load is replaced by a BPF in its ON state to accommodate for finite loading effects. Then the BPFs and diplexers are connected in a manifold configuration and their performance is co-optimized with full EM simulations in ADS and ANSYS HFSS.

III. EXPERIMENTAL VALIDATION

To validate the switchless tune-all BPF manifold concept, a prototype was designed, manufactured and tested for a wide span of frequencies in the extended FR1 band starting from

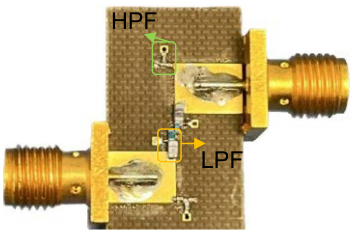

LPF
L_1: 0201DC-1N5
C_2: GJM1555C1HR80WB01
L_3: 1 nH: 0402DC-1N0

(a)

HPF
C_4: GJM1555C1HR30WB01
L_5: 0402DC-N80
C_6:GJM1555C1HR50WB01

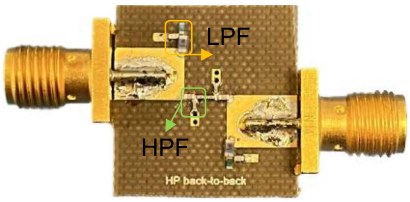

(b)

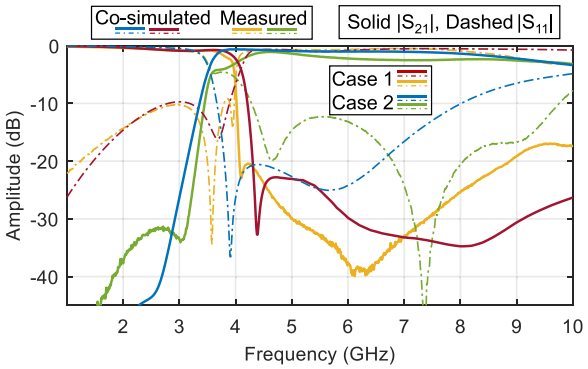

(c)

FIGURE 6. Measured and EM simulated back-to-back diplexers: (a) Case 1: LPFs: connected and HPFs: open; (b) Case 2: LPFs: open and HPFs: connected. (c) RF measured response for Case 1 and 2. .

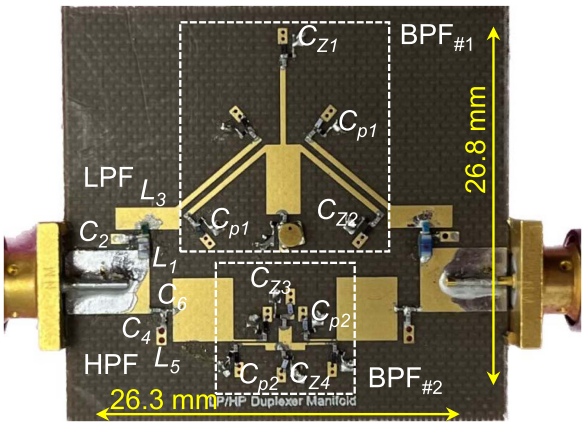

C_{P1}: MAVR-000120-14110G
C_{Z1}: MAVR-000120-14110G
C_{Z2}: MA46H071-1056
C_{block}: GRM0335C1H300JA01

r_{DC}: 10 MOhm

C_{P2}: MAVR-000120-14110G,
C_{block}: GJM1555C1HR70WB01
C_{Z1}: MAVR-000120-14110G,
C_{block}: GRM0335C1H300JA01
C_{Z2}: MAVR-000120-14110G,
C_{block}: GRM0335C1H300JA01

(a)

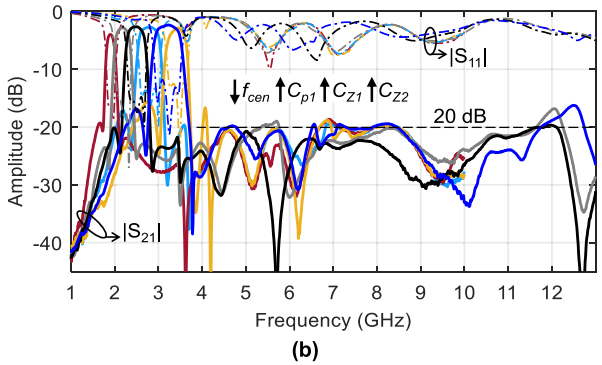

(b)

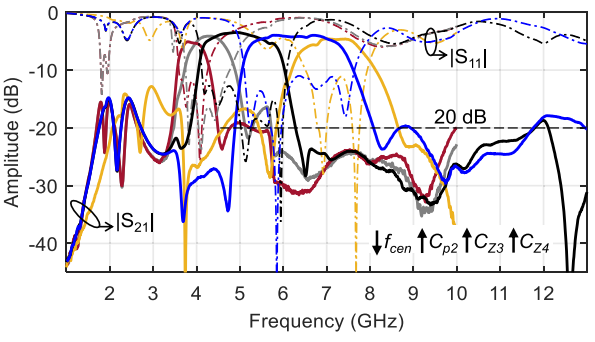

(c)

FIGURE 7. Manufactured prototype of the switchless two-BPF manifold and its RF-measured S-parameters: (a) Prototype; (b) $BPF_{\#1}$ ON exhibiting continuous f_{cen} tuning and $BPF_{\#2}$ intrinsically-switched OFF; (c) $BPF_{\#2}$ ON exhibiting continuous f_{cen} tuning with $BPF_{\#1}$ intrinsically-switched OFF.

the edge of L-band and up until C-band. The prototypes were built on RT/duroid RO5880 substrate. Test structures of the diplexers for both Case 1 and Case 2 were also manufactured and measured and are shown in Fig. 6 along with their corresponding co-simulated states. In Case 1, the insertion loss (IL) was measured < 0.8 dB for frequencies between 1–3.6 GHz, with the LPF channel cutoff at 3.97 GHz, while the out-of-band isolation was measured > 23 dB from 4.2 GHz to more than 10 GHz. In Case 2, the IL was measured < 2.4 dB for frequencies between 4.1–10 GHz, with the HPF channel cutoff at 3.76 GHz, while the out-of-band isolation was measured > 31 dB from 3.14 GHz to frequencies lower than 1 GHz. As it can be seen, the RF-measured states agree well with the EM-simulated ones. The observed small deviations are due to the lack of discrete commercially-available SMD components with the exact same optimal inductance & capacitance values specified in EM simulations.

The manufactured manifold is shown in Fig. 7(a) alongside its SMD elements. Its RF measured performance in terms of f_{cen} tuning is summarized as follows: i) Fig. 7(b): $BPF_{\#1}$ is ON

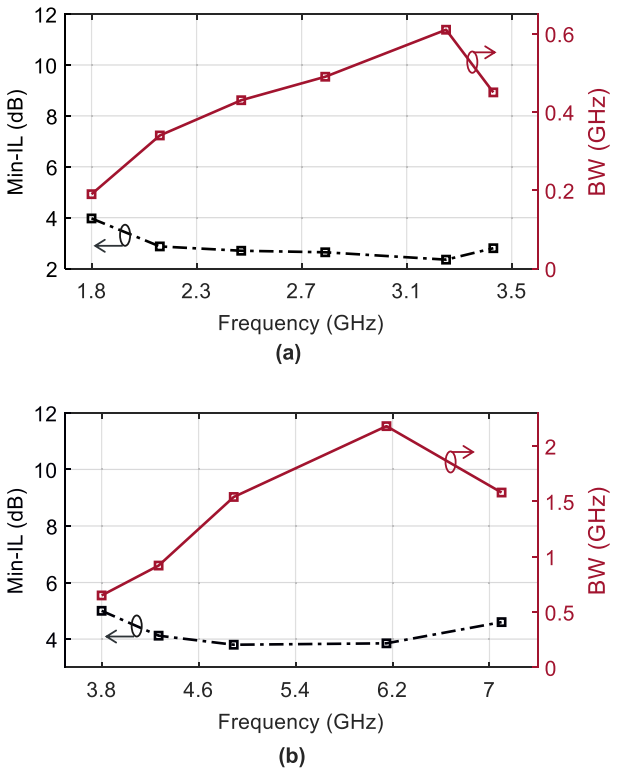

FIGURE 8. RF performance summary of the measured f_{cen} tuning states presented in Fig. 7 in terms of BW and minimum IL (min-IL): (a) $BPF_{\#1}$ f_{cen} tuning performance when $BPF_{\#2}$ is switched OFF [Fig. 7(a)]; (b) $BPF_{\#2}$ f_{cen} tuning performance when $BPF_{\#1}$ is switched OFF [Fig. 7(b)].

TABLE 1 Performance Summary for Various Tuning States When Either the $BPF_{\#1}$ or the $BPF_{\#2}$ are ON Using As a Basis the Measured Data in Fig. 7(a), (b)

	f_{cen} (GHz)	Min-BW (GHz)	Min- IL (dB)	Max-BW (GHz)	Min- IL (dB)
$BPF_{\#1}$	2.2	135	4.6	590	2.44
	3	240	3.6	725	2.3
$BPF_{\#2}$	4.9	500	5.7	1880	3.6
	6.2	695	5.1	2625	3.6

and $BPF_{\#2}$ is switched OFF and its f_{cen} is continuously tuned from 1.89 to 3.43 GHz (i.e., TR: 1.81:1). The spurious signals in the upper stopband of $BPF_{\#1}$ are naturally suppressed by the network of the LPF channel, allowing for broadband spur-free out-of-band isolation around 20 dB up to 13 GHz. ii) Fig. 7(c): $BPF_{\#2}$ is ON and $BPF_{\#1}$ is switched OFF and $BPF_{\#2}$ continuously tunes its f_{cen} from 3.8 to 7.28 GHz (i.e., TR: 1.91:1). As such, the manifold demonstrates a combined ultra-wide f_{cen} tuning between 1.89 and 7.28 GHz (i.e., TR: 3.85:1). A detailed performance summary of its measured RF f_{cen} states in terms of BW and minimum IL is provided in Fig. 8.

The BW tuning capabilities of the manifold alongside its dual-band and all-reject modes of operation are provided in Fig. 9. Namely, Fig. 9(a) shows BW tuning of $BPF_{\#1}$ ($BPF_{\#2}$ is switched OFF) at: i) f_{cen}=2.2 GHz, where its BW tunes between 0.135–0.59 GHz (i.e., a TR: 4.37:1) with a minimum IL of 2.44–4.6 dB; and at: ii) f_{cen} = 3 GHz, where its BW tunes between 0.24–0.725 GHz (i.e., a TR: 3:1) with a minimum IL between 2.3–3.6 dB. Fig. 9(b) illustrates the BW

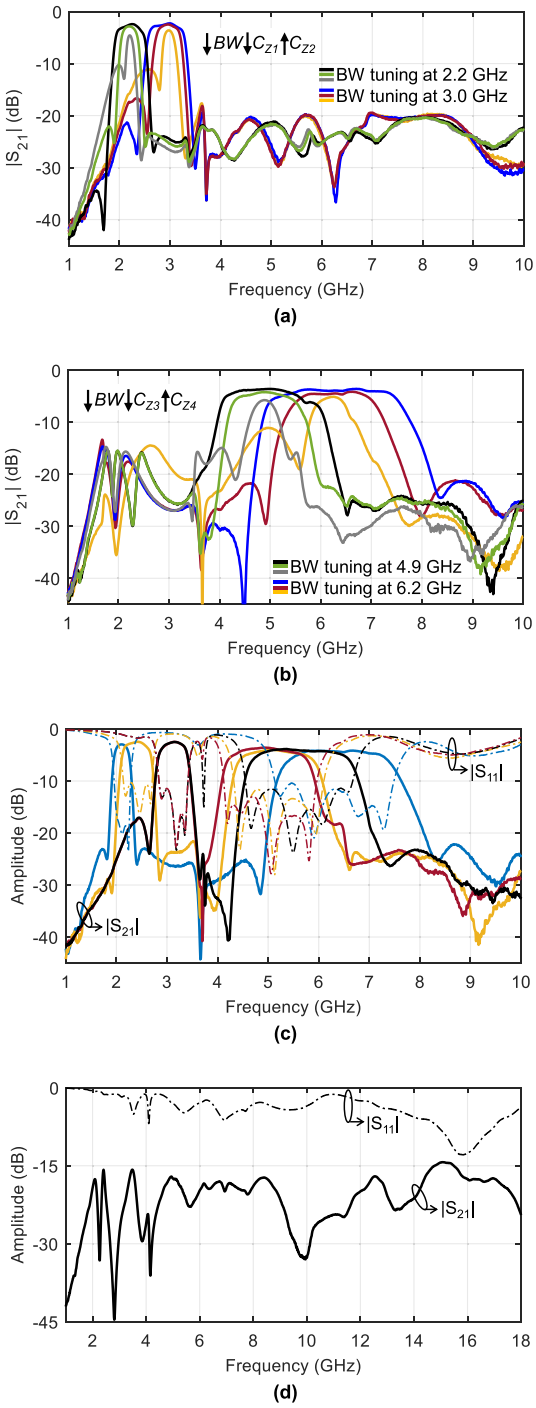

FIGURE 9. RF-measured S-parameters: (a) Continuous BW tuning of $BPF_{\#1}$ at f_{cen} = 2.2 and 3 GHz, when $BPF_{\#2}$ is OFF; (b) Continuous BW tuning of $BPF_{\#2}$ at f_{cen} = 4.9 and 6.2 GHz, when $BPF_{\#1}$ is OFF; (c) Dual-band responses when $BPF_{\#1}$ and $BPF_{\#2}$ are ON; (d) All-reject response: $BPF_{\#1}$ and $BPF_{\#2}$ are OFF.

TABLE 2 Comparison with State-of-the-Art Tunable Manifolds

Ref.	Integration	#filters	f_{cen} tuning (GHz), [TR]	FBW, TR	IL (dB)	Q_{eff}	#AE	Isolation	Operation modes
This work	**LPF/HPF diplexer**	**2**	**1.89-7.28, [3.85:1]**	**6- 42%, TR: 3- 4.7:1**	**2.3-5.7**	**12-34**	**12**	**20 dB up to 6x f_{cen}**	**Single / Dual band/ All-reject**
[9]	PIN diodes	3	0.54-2.4, [4.44]	3.4- 15%, No tuning	1.8-5.4	4.5-18.5	24	20 dB up to 5x f_{cen}	**Single** band
[11]	PIN diodes	2	1.1-2.1, [1.9:1]	1.9- 3.6%, No tuning	4.4-6.1	35-60	9	20 dB up to 2.3x f_{cen}	**Single** band
[12]	RF switch	2	1.8-3.85, [2.14]	5- 36%, TR: 2.5-3:1	2-9	11-24	14	20 dB up to 2x f_{cen}	**Single** band/ All-reject

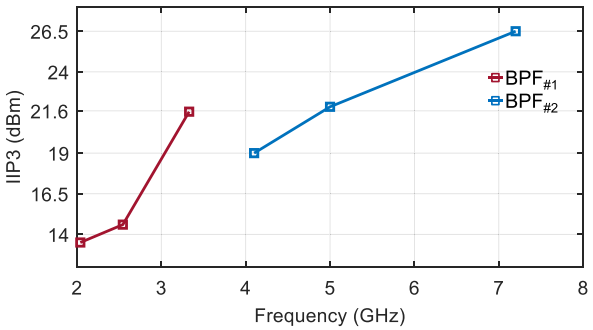

FIGURE 10. RF-measured IIP3 for various tuning states.

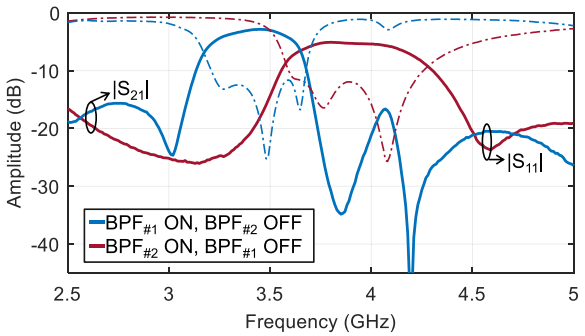

FIGURE 11. RF-measured S-parameters showing the: i) maximum f_{cen} of $BPF_{\#1}$ when $BPF_{\#2}$ is OFF and ii) minimum f_{cen} of $BPF_{\#2}$ when $BPF_{\#1}$ is OFF.

tuning capabilities of $BPF_{\#2}$ (with $BPF_{\#1}$ switched OFF) at: i) f_{cen}=4.9 GHz, where its BW tunes between 0.52–1.88 GHz (i.e., a TR: 3.6:1) with a minimum IL of 3.6–5.7 dB; and ii) f_{cen}=6.2 GHz, where its BW tunes between 0.695–2.625 GHz (i.e., a TR: 3.77:1) with a minimum IL between 3.6–5.1 dB. The RF summary of manifold BW tuning performance is listed in Table 1.

Furthermore, Fig. 9(c) demonstrates the manifold's dual-band capabilities when both $BPF_{\#1}$ and $BPF_{\#2}$ are switched ON, alongside independent f_{cen} and BW control for both of its bands. Lastly, Fig. 9(d) illustrates the measured response of the all-reject mode of operation with an isolation > 15 dB between DC and 18 GHz, achieved by intrinsically-switching OFF both $BPF_{\#1}$ and $BPF_{\#2}$.

The measured third order input intercept point (IIP3) performance of the manifold when either $BPF_{\#1}$ and $BPF_{\#2}$ are switched ON is illustrated in Fig. 10. Specifically, when $BPF_{\#1}$ is ON, an IIP3 between 13.5–21.6 dBm is obtained when f_{cen} tunes between 2–3.4 GHz. Likewise, when $BPF_{\#2\ in}$ is ON the IIP3 values ranges between 19 and 26.5 dBm when f_{cen} tunes between 4.1–7.2 GHz.

To illustrate the BPF manifold performance around the cross-over region of the diplexer, Fig. 11 provides the RF-measured response of: i) the maximum f_{cen} state of $BPF_{\#1}$ when $BPF_{\#2}$ is switched OFF and ii) the minimum f_{cen} state of $BPF_{\#2}$ when $BPF_{\#1}$ is switched OFF. The upper 3-dB frequency of $BPF_{\#1}$ is 3.64 GHz (blue trace), while the lower 3-dB frequency of $BPF_{\#2}$ is 3.59 GHz (red trace). Therefore, the BPF manifold allows complete frequency coverage between 1.89– 7.28 GHz.

To demonstrate the potential of the proposed switchless BPF manifold for ultra-wide and tune-all RF tuning in FR1, a comparison with state-of-the-art tunable manifolds is presented in Table 2. As shown, the proposed configuration is the only RF-switchless manifold to date covering the highest operational frequency, while exhibiting ultra-wide f_{cen} tuning and BW tuning and supporting the largest number of modes of operation namely single, dual-band, and all-reject modes of operation. Furthermore, it exhibits the lowest IL and the widest out-of-band suppression with > 20 dB of isolation for up to 6xf_{cen}. The concepts in [9], [11] are only tunable in terms of f_{cen} and the manifold in [12], doesn't facilitate a dual-mode of operation, it has significantly higher IL up to 9 dB and can only operate up to 3.85 GHz.

VII. CONCLUSION

A novel switchless tune-all two-BPF manifold design is presented. It is based on two LPF/HPF diplexer junctions and two tune-all, intrinsically-switchable BPFs. The manifold exhibits ultra-wide and highly-versatile transfer function characteristics with three modes of operation, namely: i) a single-band BPF with 3.85:1 f_{cen} tuning, up to 4.4:1 BW tuning, and > 20 dB out-of-band isolation; ii) a dual-band BPF with two independently tuned bands; and iii) an all-reject mode with > 15 dB isolation between DC and 18 GHz.

ACKNOWLEDGMENT

Distribution Statement A. Approved for Public Release, Distribution Unlimited. The views, opinions and/or findings

expressed are those of the authors and should not be interpreted as representing the official views or policies of the Department of Defense or the U.S. Government.

REFERENCES

[1] W. J. Chappell, E. J. Naglich, C. Maxey, and A. C. Guyette, "Putting the radio in 'software-defined radio': Hardware developments for adaptable RF systems," *Proc. IEEE*, vol. 102, no. 3, pp. 307–320, Mar. 2014.

[2] T. Lim, A. Anand, J. Chen, X. Liu, and Y. Lee, "Design method for tunable planar bandpass filters with single-bias control and wide tunable frequency range," *IEEE Trans. Circuits Syst. II, Exp. Briefs*, vol. 68, no. 1, pp. 221–225, Jan. 2021.

[3] M. Fan, K. Song, L. Yang, and R. Gomez-Garcia, "Frequency-tunable constant-absolute-bandwidth single-/dual-passband filters and diplexers with all-port-reflectionless behavior," *IEEE Trans. Microw. Theory Techn.*, vol. 69, no. 2, pp. 1365–1377, Feb. 2021.

[4] J. Xu, L. Yang, Y. Yang, and X. Y. Zhang, "High-Q-factor tunable bandpass filter with constant absolute bandwidth and wide tuning range based on coaxial resonators," *IEEE Trans. Microw. Theory Techn.*, vol. 67, no. 10, pp. 4186–4195, Oct. 2019.

[5] D. Lu, M. Yu, N. S. Barker, Z. Li, W. Li, and X. Tang, "Advanced synthesis of wide-tuning-range frequency-adaptive bandpass filter with constant absolute bandwidth," *IEEE Trans. Microw. Theory Techn.*, vol. 67, no. 11, pp. 4362–4375, Nov. 2019.

[6] Q. Xiang, H. Sun, M. Fu, Q. Jin, and Q. Feng, "A 5th-order constant bandwidth tunable bandpass filter with two cascaded trisection structures," *IEEE Trans. Circuits Syst. II, Exp. Briefs*, vol. 70, no. 1, pp. 126–130, Jan. 2023.

[7] Z. Li, X. Tang, D. Lu, Z. Cai, Y. Liu, and J. Luo, "Lowloss wide-tuning-range three-pole frequency-agile bandpass diplexer with identical constant absolute bandwidth," *IEEE Access*, vol. 7, pp. 149833–149845, 2019.

[8] M. A. El-Tanani and G. M. Rebeiz, "Corrugated microstrip coupled lines for constant absolute bandwidth tunable filters," *IEEE Trans. Microw. Theory Techn.*, vol. 58, no. 4, pp. 956–963, Apr. 2010.

[9] C. F. Chen, "Design of a microstrip three-state switchable and fully tunable bandpass filter with an extra-wide frequency tuning range," *IEEE Access*, vol. 8, pp. 66438–66447, 2020.

[10] J. S. Sun, N. Kaneda, Y. Baeyens, T. Itoh, and Y. K. Chen, "Multilayer planar tunable filter with very wide tuning bandwidth," *IEEE Trans. Microw. Theory Techn.*, vol. 59, no. 11, pp. 2864–2871, Nov. 2011.

[11] C. F. Chen, G. Y. Wang, and J. J. Li, "Microstrip switchable and fully tunable bandpass filter with continuous frequency tuning range," *IEEE Microw. Wireless Compon. Lett.*, vol. 28, no. 6, pp. 500–502, Jun. 2018.

[12] M. R. A. Nasser, R. K. Jaiswal, and D. Psychogiou, "A compact bandpass filter manifold with ultrawide frequency and bandwidth tuning," *IEEE Access*, vol. 11, pp. 41054–41060, 2023.

[13] S. Shin, E. Naglich, and L. Boglione, "Back-to-back connected multiplexers for a broadband channel splitter and channel combiner," in *Proc. IEEE 49th Eur. Microw. Conf.*, Paris, France, 2019, pp. 188–191.

[14] Skyworks Solutions Inc., "SKYA21003: 0.1 to 8.5 GHz SPDT Switch," 202938K datasheet, Dec. 2022.

MOHAMMED R. A. NASSER (Graduate Student Member, IEEE) received the electrical engineering from The Islamic University of Gaza, Gaza, Palestine, in 2017, and the master's degree in electrical engineering from Akdeniz University, Antalya, Türkiye, in 2020. He is currently a Graduate Student with the Tyndall National Institute and the School of Engineering, University College Cork, Cork, Ireland. He is a Member of the IEEE Microwave Theory and Techniques Society. His research interests include designing reconfigurable planar and acoustic-resonator-based RF/microwave filters.

DIMITRA PSYCHOGIOU (Senior Member, IEEE) received the Dipl.-Eng. degree in electrical and computer engineering from the University of Patras, Patras, Greece, in 2008, and the Ph.D. degree in electrical engineering from the Swiss Federal Institute of Technology (ETH), Zürich, Switzerland, in 2013. She was a Sr. Research Scientist with Purdue University, West Lafayette, IN, USA, and an Assistant Professor with the University of Colorado Boulder, Boulder, CO, USA. She is currently a Professor of electrical and electronic engineering with the University College Cork, Cork, Ireland, and the Head of the Advanced RF Technology Group, Tyndall National Institute, Cork, Ireland. Her research interests include RF design and characterization of reconfigurable microwave and millimeter-wave passive components, RF-MEMS, acoustic wave resonator-based filters, tunable filter synthesis, frequency-agile antennas, and additive manufacturing technologies for 3D antenna sub-systems. Her research has been presented in more than 230 publications and has received multiple awards including the 2023 IEEE MTT-S Outstanding Young Engineer Award, 2021 Roberto Sorrentino Prize, SFI Research Professorship Award, 2020 NSF CAREER Award, 2020 URSI Young Scientist Award, and Junior Faculty Outstanding Research Award from UC Boulder. She is a Senior Member of URSI and a Member of IEEE MTT-S Filters and Passive Components (MTT-5) and Microwave Control Materials and Devices (MTT-13) committees. She serves on the Technical Review Board of various IEEE and EuMA conferences and journals. She is the Chair of MMT-13 and Secretary of USNC-URSI Commission. She is an Associate Editor for IEEE MICROWAVE AND WIRELESS COMPONENTS LETTERS and *International Journal of Microwave and Wireless Technologies*. She was an Associate Editor of *IET Microwaves, Antennas and Propagation Journal*.